Journal of Applied Physics

RESEARCH ARTICLE | SEPTEMBER 25 2014

Electrical control of a single magnetoelastic domain structure on a clamped piezoelectric thin film—analysis

Cheng-Yen Liang; Scott M. Keller; Abdon E. Sepulveda; Wei-Yang Sun; Jizhai Cui; Christopher S. Lynch; Gregory P. Carman

J. Appl. Phys. 116, 123909 (2014)
https://doi.org/10.1063/1.4896549

AIP Publishing

JOURNAL OF APPLIED PHYSICS **116**, 123909 (2014)

Electrical control of a single magnetoelastic domain structure on a clamped piezoelectric thin film—analysis

Cheng-Yen Liang, Scott M. Keller, Abdon E. Sepulveda, Wei-Yang Sun, Jizhai Cui, Christopher S. Lynch, and Gregory P. Carman
Department of Mechanical and Aerospace Engineering, University of California, Los Angeles, California 90095, USA

(Received 28 April 2014; accepted 12 September 2014; published online 25 September 2014)

This paper presents an analytical model coupling Landau-Lifshitz-Gilbert micromagnetics with elastodynamics and electrostatics to model the response of a single domain magnetoelastic nano-element attached to a piezoelectric thin film (500 nm). The thin film piezoelectric is mounted on a Si substrate, globally clamping the film from in-plane extension or contraction. Local strain transfer to the magnetoelastic element is achieved using patterned electrodes. The system of equations is reduced to eight coupled partial differential equations as a function of voltage (V), magnetic potential ϕ, magnetic moments ($\underline{m}$), and displacements ($\underline{u}$), i.e., fully coupled material. The weak forms of the partial differential equations are solved using a finite element formulation. The problem of a Ni single domain structure (i.e., 150 nm × 120 nm × 10 nm) on a thin film (500 nm) piezoelectric transducer (PZT)-5H attached to an infinite substrate is studied. Discretization in the single domain structure is on the order of the exchange length (8.5 nm), providing spatial and temporal information on the local mechanical and magnetic fields. A -0.5 V potential is applied to a pair of surface electrodes, producing out-of-plane deformation and in turn straining the magnetoelastic single domain nanostructure in-plane. This strain is sufficient to reorient a single domain structure representative of an idealized memory element.
[http://dx.doi.org/10.1063/1.4896549]

I. INTRODUCTION AND BACKGROUND

For the past decade, researchers have focused on developing a magnetic memory element using a multiferroic material.[1] One approach uses a strain-mediated composite approach consisting of layered piezoelectric and magnetoelastic materials strain coupled together.[2–4] Researchers have analytically shown that the energy required to reorient/write a single magnetic domain structure can be very small, i.e., considerably smaller than conventional approaches to writing bits of memory.[5–8] However, the multiferroic composite memory element is typically fabricated on a fairly thick substrate system, e.g., silicon. This thick substrate clamps the piezoelectric/magnetoelastic material, limiting the amount of strain that can be generated, posing a significant challenge for the implementation of a strain-mediated memory element. In this analytical work, we demonstrate a concept to overcome the substrate clamping issue and show reorientation of a magnetic single domain between two stable states by simply pulsing the voltage.

Previous researchers have demonstrated the control of the magnetization states in thin film magnetoelastic material deposited on a thick piezoelectric substrate.[9–13] This effect has been used to alter magnetic domains[2,3,10,11] and to shift the magnetic coercive field.[12,13] As an alternative to using in-plane polarized piezoelectric material, some researchers such as Wu used the auxetic piezoelectric strain produced by [011] cut $[\mathrm{Pb(Mg_{1/3}Nb_{2/3})O3}]_{(1-x)}$-$[\mathrm{PbTiO_3}]_x$ (PMN-PT, $x \approx 0.32$) (PMN-PT), while others have used the same effect in $\mathrm{Pb(Zn_{(1/3)}Nb_{(2/3)})O_{(3-x)}PbTiO_{(3)}}$ single crystals.[14,15] These single crystal approaches resulted in a proposed design of a magnetoelectric memory system, but once again still required bulk piezoelectric material.[5,16] Moutis *et al.* in 2008 reported electric-field modulation of coercive field H_c using periodic arrays of ferromagnetic (FM) $\mathrm{Co_{50}Fe_{50}}$ stripes.[17] Bur *et al.* in 2011 reported strain-induced coercive field changes in patterned single-domain nickel nanostructures deposited on a thick $\mathrm{Si/SiO_2}$ substrate using external mechanical loads,[18] while Nan *et al.* suggested single domain reorientation on bulk PMN-PT single crystal.[5] Regarding piezoelectric materials deposited onto a substrate, out-of-plane magnetic reorientation has been achieved with magnetic beat frequency oscillator (BFO)/$\mathrm{CoFe_2O_4}$ vertical nanoscale structures embedded in a ferroelectric thin film, as described by Zavaliche *et al.* in 2005, but this approach is non-deterministic.[19] Chung *et al.* studied single domain elements on a thin film piezoelectric, but did not demonstrate reorientation of the magnetic domain.[10,11] None of these studies provides an acceptable approach to reorient a single domain structure deterministically using strain-mediated approach on a constrained substrate.

The development of a strain-mediated multiferroic memory device requires the magnetization of each element to be individually controllable using a ferroelectric thin film grown on a substrate (e.g., Si wafer). The problem with this concept it that the thin film piezoelectric is clamped by the thick substrate and prevents strain transfer. Cui *et al.* suggested the use of patterned electrodes to overcome substrate clamping and obtain highly localized strain in both the thin film piezoelectric and the magnetic material.[20] The general concept was demonstrated on a bulk piezoelectric ceramic, but did not include detailed analysis (or experiments) for a thin film piezoelectric.

The analysis of single domain switchable magnetoelectric heterostructures requires the use of the Landau-Lifshitz-Gilbert (LLG) micromagnetic approaches developed in the 1950s.[21] An important addition to micromagnetics was the inclusion of strain (or stress) for magnetostrictive materials by Zhu *et al*. in 2001.[22] This was used by Hu in 2006 to model the effect of stress on hysteresis curves and magnetization dynamics, showing the interaction of stress with coercivity and the easy axis of magnetoelastic materials.[23] Building on these advancements, Hu *et al*. used stability conditions and proposed an electric field read and write MERAM device.[6] A balance of both shape and strain anisotropy was used to describe an elliptical nanomagnet that could be switched under stress by Roy *et al*.[7] In most of these studies, however, magnetization and strain were assumed to be spatially homogeneous and thus the clamping issues produced by the substrate were not addressed. D'Souza *et al*. in 2011 proposed and analyzed a low-power 4-state universal logic gate using a linear array of multiferroic nanomagnets, but did not consider the substrate clamping issue.[24] Tiercelin *et al*. described and analyzed a magnetoelectric memory cell that balanced strain anisotropy, shape anisotropy, and a bias field.[8] In this later work, the elastic contribution was modeled separately and the piezoelectric film was not attached to a substrate.

In this paper, a single domain magnetoelastic elliptical nanostructure deposited onto a thin film piezoelectric wafer attached to a thick substrate is modeled by coupling micromagnetics (LLG), elastodynamic, and electrostatics partial differential equations. The nickel magnetoelastic ellipse (150 nm × 120 nm × 10 nm) has shape anisotropy and an applied magnetic field along the minor axis to shift the energy wells, as described originally by Tiercelin in 2011.[8] The thin film (500 nm) piezoelectric is attached to a thick substrate that clamps and prevents relative in-plane motion of the piezoelectric at the interface of the film with the substrate. Four electrodes are placed around the Ni magnetoelastic element similar to Tiercelin;[8] however, these electrodes produce out-of-plane electric fields rather than in-plane electric fields,[20] and the thin film is mounted onto a substrate. The intrinsic coupling of the piezoelectric response with the magnetoelastic response through strain is modeled by coupled partial differential equations (i.e., electrostatics tied to micromagnetics while solving elastodynamics). The numerical formulation uses tetrahedral finite elements with a maximum size equal to the exchange length of nickel (~8.5 nm), providing spatially varying strains, electric fields, and magnetic spins throughout the structure. Therefore, the model captures all the relevant physics required to accurately predict the response of this multiferroic nanoscale structure and demonstrates single domain magnetic reorientation in a strain-mediated structure attached to a thick clamped substrate.

II. THEORY FOR COMPUTATIONAL MODEL

Strain-mediated multiferroic composites consist of both piezoelectric and magnetoelastic materials. Thus, the fundamental governing equations for predicting the dynamic response are based on electrostatics, micromagnetics (LLG), and elastodynamics. In this paper, the general governing equations for a strain-mediated electro-mechanical and magnetoelastic materials are derived from which individual phases represent limiting cases. The following derivation presents a general approach for developing the governing equations in weak forms, which are then implemented into a finite element formulation. Assumptions include small elastic deformations, linear elasticity, linear piezoelectricity, electrostatics, and negligible electrical current contributions. The single general derivation presented can be subsequently decoupled to predict the response of an electro-mechanical or magnetoelastic material.

The strain for a multiferroic (magneto-electric-elastic) material is given by

$$\underline{\underline{\varepsilon}} = \underline{\underline{\varepsilon}}^{el} + \underline{\underline{\varepsilon}}^{PE} + \underline{\underline{\varepsilon}}^{m}(\underline{m}), \tag{1}$$

where $\underline{\underline{\varepsilon}}$ is the total strain with contributions from the elastic strain $\underline{\underline{\varepsilon}}^{el} = \underline{\underline{\underline{C}}}^{-1}\underline{\underline{\sigma}}$, the piezoelectric strain $\underline{\underline{\varepsilon}}^{PE} = \underline{\underline{\underline{d}}}\,\underline{E}$, and the magnetostriction strain $\underline{\underline{\varepsilon}}^{m} = \underline{\underline{\underline{\bar{\lambda}}}}^{m}\underline{mm^{T}}$. Here, $\underline{\underline{\underline{C}}}$ is the elastic stiffness tensor, $\underline{\underline{\sigma}}$ is the stress tensor, $\underline{\underline{\underline{d}}}$ is the piezoelectric strain tensor, $\underline{E}$ is the electric field vector, $\underline{\underline{\underline{\lambda}}}$ is the magneto-mechanical coupling tensor, and $\underline{m} = \frac{\underline{M}}{M_s}$ is the normalized local magnetization vector with M_s, representing saturation magnetization. For a cubic crystal, the components of $\underline{\underline{\varepsilon}}^{m}$ in a cubic referenced coordinate system are given by

$$\varepsilon_{ij}^{m} = \begin{cases} \dfrac{3}{2}\lambda_{100}\left(m_i m_j - \dfrac{1}{3}\right) & i = j \\ \dfrac{3}{2}\lambda_{111} m_i m_j & i \neq j, \end{cases} \tag{2}$$

where λ_{100} and λ_{111} are magnetostriction constants along the $\langle 100 \rangle$ and $\langle 111 \rangle$ directions.[25–29] For hexagonal or uniaxial crystals, Eq. (2) would have a different form that can easily be implemented in the approach;[28] and for an isotropic polycrystalline, the two coefficients have the same value.

The electrical portion of the constitutive equation, assuming negligible magnetic and electric field coupling, is given by

$$\underline{D} = \underline{\underline{\underline{d}}}^{T}\underline{\underline{\sigma}} + \underline{\underline{\varepsilon_s}}\,\underline{E}, \tag{3}$$

where $\underline{\underline{\varepsilon_s}}$ is the dielectric tensor and $\underline{D}$ is the electric displacement. For a general multiferroic material, an additional term would appear in Eq. (3), representing the coupling between magnetic and electric fields; but for this derivation, we have assumed this component is negligible. The coupling between magnetic and electric fields in the material modeled in this paper arises due to the stress term in Eq. (3) and its coupling to magnetic strain presented in Eq. (1). The electrostatic governing equations are

$$\nabla \cdot \underline{D} = \rho_f, \quad \underline{E} = -\nabla V, \tag{4}$$

where V is the electric potential and ρ_f is density of free charges. The electric potential V is obtained by combining Eqs. (3) and (4) for electrostatic behavior ($\rho_f = 0$)

$$\nabla\cdot[\underline{\underline{d}}^{T}\underline{\underline{\sigma}}+\varepsilon_{s}(-\nabla V)]=0. \tag{5}$$

The magnetic response of the multiferroic media is governed by the phenomenological LLG micromagnetic relation

$$\frac{\partial \underline{m}}{\partial t}=-\mu_{0}\gamma(\underline{m}\times\underline{H}_{eff})+\alpha\left(\underline{m}\times\frac{\partial \underline{m}}{\partial t}\right), \tag{6}$$

where μ_0 is the permeability in the vacuum, γ is the Gilbert gyromagnetic ratio, and α is the Gilbert damping constant.[21] $\underline{H}^{eff}$ is the effective magnetic field, which is obtained from the total energy density and is given by

$$\begin{aligned}\underline{H}_{eff}&=-\frac{1}{\mu_0 M_S}\frac{\partial E_{tot}}{\partial \underline{m}}\\&=\underline{H}_{ext}+\underline{H}_{ex}+\underline{H}_{anis}+\underline{H}_{d}+\underline{H}_{me}(\underline{m},\underline{u}(\underline{E})),\end{aligned} \tag{7}$$

where E_{tot} is the total energy density, which includes the Zeeman energy density due to an applied external field, the exchange energy density, the magnetocrystalline anisotropy energy density, the demagnetization energy density, and the elastic energy density.[21,25,26] $\underline{H}_{ext}$ is the applied external field, $\underline{H}_{ex}$ is the exchange field, $\underline{H}_{anis}$ is the anisotropic field, $\underline{H}_{d}$ is the demagnetization field, and $\underline{H}_{me}$ is the magnetoelastic field. Expressions for these terms follow:

$$\underline{H}_{ex}=\frac{2A_{ex}}{\mu_0 M_s}\nabla^{2}\underline{m}, \tag{8.1}$$

$$H^{i}_{anis}=-\frac{2m_i}{\mu_0 M_S}\left[K_1\left(m_j^2+m_k^2\right)+K_2\left(m_j^2 m_k^2\right)\right], \tag{8.2}$$

where K_1 and K_2 are cubic anisotropy constants.[21,25,26,29] The equation for the anisotropy field H^{i}_{anis} will take a different form for other crystal symmetries. The demagnetization field $\underline{H}_{d}$ is determined from Ampere's law ($\nabla\times\underline{H}_{d}=0$), Gauss's law ($\nabla\cdot\underline{B}=0$), and the relation between the magnetic induction $\underline{B}$ and magnetization $\underline{m}$:

$$\underline{B}=\underline{H}_{d}+M_{s}\underline{m}. \tag{9}$$

$\underline{H}_{d}$ is expressed as the gradient of a magnetic potential ϕ by using Ampere's law,[31,32]

$$\underline{H}_{d}=-\nabla\phi. \tag{10}$$

Using Gauss's law with Eqs. (9) and (10), the magnetic potential ϕ satisfies the Poisson equation,[31]

$$\nabla^{2}\phi=\nabla\cdot(M_{s}\underline{m}). \tag{11}$$

The magnetoelastic field is obtained by differentiating the elastic energy density in Eq. (7)[29]

$$\underline{H}_{me}=-\frac{1}{\mu_0 M_S}\underline{\underline{\underline{C}}}(\underline{\underline{\varepsilon}}-\underline{\underline{\varepsilon}}^{m}(\underline{m})-\underline{\underline{\varepsilon}}^{PE}(\underline{E}))\cdot\partial\frac{\underline{\underline{\varepsilon^{m}(\underline{m})}}}{\partial\underline{m}}. \tag{12}$$

The mechanical response of the is governed by the elastodynamic equation

$$\rho\frac{\partial^{2}\underline{u}}{\partial t^{2}}-\nabla\cdot\underline{\underline{\sigma}}=\underline{0}, \tag{13}$$

where ρ is the mass density. The total strain $\underline{\underline{\varepsilon}}$ from Eq. (1) is related to the displacement $\underline{u}$ vector[29] as

$$\underline{\underline{\varepsilon}}=\frac{1}{2}\left(\nabla\underline{u}+(\nabla\underline{u})^{T}\right) \tag{14}$$

and the stress tensor $\underline{\underline{\sigma}}$ is related to the strains[29] as

$$\underline{\underline{\sigma}}=\underline{\underline{\underline{C}}}\,\underline{\underline{\varepsilon}}^{el}=\underline{\underline{\underline{C}}}[\underline{\underline{\varepsilon}}-\underline{\underline{\varepsilon}}^{m}(\underline{m})-\underline{\underline{\varepsilon}}^{PE}(\underline{E})]. \tag{15}$$

Equations (1)–(15) represent a system of equations describing the electro-magneto-mechanical response. Substituting Eqs. (14) and (15) and the expression for $\underline{\underline{\varepsilon}}^{m}(\underline{m})$ into Eq. (13) results in a modified elastodynamic partial differential equation in terms of displacements $\underline{u}$, electric field $\underline{E}$, and magnetization $\underline{m}$,[26]

$$\begin{aligned}\rho\frac{\partial^{2}\underline{u}}{\partial t^{2}}&-\nabla\cdot\underline{\underline{\underline{C}}}\left[\frac{1}{2}\left(\nabla\underline{u}+(\nabla\underline{u})^{T}\right)\right]\\&+\nabla\cdot\underline{\underline{\underline{C}}}\left(\underline{\underline{\underline{\lambda}}}^{m}\underline{mm}^{T}\right)+\nabla\cdot\underline{\underline{\underline{C}}}\left(\underline{\underline{d}}\,\underline{E}\right)=\underline{0},\end{aligned} \tag{16}$$

where the electric field E is obtained from Eq. (4). Note that the partial differential equation is fully coupled with electric ($\underline{E}(V)$), magnetic ($\underline{m}$), and mechanical displacement fields ($\underline{u}$); thus a fully coupled multiferroic material is modeled. Combining Eqs. (6) and (7) produces the modified LLG equation in terms of displacements ($\underline{u}$), electric field ($\underline{E}$), and magnetization ($\underline{m}$):

$$\begin{aligned}\frac{\partial\underline{m}}{\partial t}=&-\mu_0\gamma(\underline{m}\times(\underline{H}_{ext}+\underline{H}_{ex}(\underline{m})+\underline{H}_{d}(\phi)\\&+\underline{H}_{anis}(\underline{m})+\underline{H}_{me}(\underline{m},\underline{u}(\underline{E}))))+\alpha\left(\underline{m}\times\frac{\partial\underline{m}}{\partial t}\right).\end{aligned} \tag{17}$$

Equations (5), (11), (16), and (17) represent eight fully coupled partial differential equations for the eight unknown variables represented by V, $\underline{u}$, ϕ, and $\underline{m}$. In this paper, the coupled partial differential equations are formulated in their weak forms. The weak form of Eq. (5) is obtained by multiplying it by test functions β, which satisfy boundary conditions, and then integrating over the volume Ω. Using the divergence theorem[31] gives

$$\begin{aligned}&\int_{\Omega}\left(\varepsilon_s-\underline{\underline{d}}\,\underline{\underline{\underline{C}}}\,\underline{\underline{d}}^{T}\right)(-\nabla V)\frac{\partial\beta}{\partial\underline{x}}d\Omega\\&+\int_{\Omega}\left(\underline{\underline{d}}^{T}\underline{\underline{\underline{C}}}\left(\frac{1}{2}\left(\nabla\underline{u}+(\nabla\underline{u})^{T}\right)-\underline{\underline{\underline{\lambda}}}^{m}\underline{mm}^{T}\right)\right)\frac{\partial\beta}{\partial\underline{x}}d\Omega\\&=\int_{S}\left(\varepsilon_s-\underline{\underline{d}}\,\underline{\underline{\underline{C}}}\,\underline{\underline{d}}^{T}\right)(-\nabla V)\beta n dS\\&+\int_{S}\left(\underline{\underline{d}}^{T}\underline{\underline{\underline{C}}}\left(\frac{1}{2}\left(\nabla\underline{u}+(\nabla\underline{u})^{T}\right)-\underline{\underline{\underline{\lambda}}}^{m}\underline{mm}^{T}\right)\right)\beta n dS\end{aligned} \tag{18}$$

with the following prescribed electric potential boundary conditions

$$V=V_{0}\ \text{on}\ S, \tag{19}$$

where V_0 is the electric potential on the surface S. The weak form of Eq. (11) is obtained by using a test functions ζ[31] giving

$$-\int_{\Omega}(\nabla\phi)\frac{\partial\zeta}{\partial\underline{x}}d\Omega+\int_{\Omega}(M_s\underline{m})\frac{\partial\zeta}{\partial\underline{x}}d\Omega + \int_{S}(-\nabla\phi+M_s\underline{m})\zeta n dS=0. \tag{20}$$

With the following prescribed magnetic potential boundary conditions,[31]

$$\begin{cases}\phi_{in}=\phi_{out} \\ \dfrac{\partial\phi_{in}}{\partial n}-\dfrac{\partial\phi_{out}}{\partial n}=-(M_s\underline{m})\cdot n\end{cases} \text{on } S, \tag{21}$$

where ϕ_{in} and ϕ_{out} are the inner and outer magnetic potentials and n is the unit normal to the surface S. Similarly, the weak formulation for Eq. (16) is obtained by using test vector functions η,[34,36] producing

$$\begin{aligned}&\int_{\Omega}\left(\rho\frac{\partial^2\underline{u}}{\partial t^2}\right)\cdot\underline{\eta}\,d\Omega+\int_{\Omega}\nabla\underline{\eta}\cdot\left(\underline{\underline{\underline{\underline{C}}}}\left[\frac{1}{2}\left(\nabla\underline{u}+(\nabla\underline{u})^T\right)\right]\right)d\Omega \\ &+\int_{\Omega}\left[\underline{\underline{\underline{\underline{C}}}}\left(\underline{\underline{\underline{\underline{\lambda}}}}^{m}\underline{mm}^T\right)+\underline{\underline{\underline{\underline{C}}}}\left(\underline{\underline{\underline{d}}}(-\nabla V)\right)\right]\nabla\underline{\eta}d\Omega \\ &=\int_{S}\underline{\eta}\cdot\underline{\underline{\underline{\underline{C}}}}\left[\frac{1}{2}\left(\nabla\underline{u}+(\nabla\underline{u})^T\right)-\left(\underline{\underline{\underline{\underline{\lambda}}}}^{m}\underline{mm}^T\right)-\left(\underline{\underline{\underline{d}}}(-\nabla V)\right)\right]\cdot ndS\end{aligned} \tag{22}$$

with prescribed displacements and prescribed tractions on the corresponding boundaries,

$$\underline{u}=\underline{u}^0 \text{ on } S_1, \tag{23.1}$$

$$\underline{\underline{\sigma}}\cdot\hat{n}=\underline{t} \text{ on } S_2, \tag{23.2}$$

where S_1 and S_2 are sub-boundaries on S ($S_1\cup S_2=S$). Finally, to construct the weak form of Eq. (17), the vector test function $\underline{\psi}$ is used to produce[33,34]

$$\begin{aligned}&\int_{\Omega}\left(\frac{\partial\underline{m}}{\partial t}-\alpha\left(\underline{m}\times\frac{\partial\underline{m}}{\partial t}\right)\right)\cdot\underline{\psi}\,d\Omega \\ &=-\int_{\Omega}\mu_0\gamma(\underline{m}\times(\underline{H}_{ext}+\underline{H}_d+\underline{H}_{anis}+\underline{H}_{me}))\cdot\underline{\psi}d\Omega \\ &+\frac{2A_{ex}\gamma}{M_s}\sum_{l}\int_{\Omega}\left(\underline{m}\times\frac{\partial\underline{m}}{\partial x_l}\right)\cdot\frac{\partial\psi_l}{\partial x_l}d\Omega\end{aligned} \tag{24}$$

with the boundary condition[21,33,34]

$$\frac{\partial\underline{m}}{\partial n}=0 \text{ on } S \tag{25}$$

and subject to the constraint

$$|\underline{m}|=1 \text{ on } \Omega, \tag{26}$$

which is a direct consequence of the LLG equation.[21,33,34] Finally, Eqs. (18), (20), (22), and (24) in addition to the boundary conditions given in Eqs. (19), (21), (23), and (25) represent a well-posed problem that can be solved using finite element methods.

The weak forms are solved using the finite element method with an implicit time stepping scheme and backward differentiation formula (BDF).[35] To decrease solution time, the system of equations is solved using a segregated solution approach, which splits the solution process into substeps using a damped Newton's method. For all numerical problems, convergence studies (i.e., mesh size and time steps) were conducted to ensure accuracy. The time step is 5×10^{-11} s and duration is 2×10^{-12} s.[35]

III. RESULTS

Prior to showing analytical results, we first describe the physical mechanism of deterministically reorienting the magnetization in a single domain element by 90° using magnetoelastic properties.[8] Figure 1 shows the energy profiles as a function of the magnetization angle for two different nanoscale geometries (~100 nm, in-plane 10 nm thick), i.e., a circular Figure 1(a) or elliptical disk Figure 1(b). For a circular disk, as shown in Figure 1(a), there are no preferential magnetic energy wells, thus the in-plane magnetization direction is independent of angle. For an elliptical disk, as shown in Figure 1(b), there are two energy minima aligned along the major axis at 0 and 180°. By introducing a magnetic bias field (H_b) aligned along the ellipse's minor axis (see Figure 1(c)), the angle between the energy wells decreases, i.e., from 0/180 in Figure 1(b) to 45/135 in Figure 1(c) with H_b applied. The simultaneous application of a magnetic field and a mechanical strain to the magnetoelastic ellipse (e.g., negative magnetostriction), as shown in Figures 1(d) and 1(e), modifies the two energy wells magnitude relative to each other rather than substantially change the angle (i.e., 45/135). This approach, i.e., application of a constant magnetic bias field with the application and removal of a mechanical strain, allows deterministic strain-mediated switching between two stable states.[8]

Figure 2 shows an illustration of the analytical model to demonstrate reorientation of a Ni magnetoelastic ellipse. The 500 nm piezoelectric transducer (PZT)-5H thin film has a Pt bottom ground electrode deposited onto a 0.5 mm thick Si substrate. The PZT-5H is represented with linear piezoelectric elements (i.e., subset of derived model) for this region. While not shown in Figure 2(a), an exchange layer could be used between the Pt and Ni structures for applying the bias field in-situ (i.e., following the concept introduced in Figures 1(d) and 1(e)).[38] Figure 2(a) shows the 150 nm × 120 nm × 10 nm Ni ellipse surrounded by four 125 nm × 125 nm × 10 nm Au electrodes. The Ni is represented with nonlinear magnetoelastic elements, while the Au is represented with linear mechanics elements (i.e., both subsets of the derived model). The two electrodes A-A are at a 45° angle, and the two electrodes B-B are at a 135° angle relative to the major axis of the ellipse (i.e., x-direction). The PZT-5H film is poled through the thickness in the z direction. The model presented in Figure 2 for the Ni ellipse, the electrodes, and the PZT-5H film thickness have not been optimized for a given objective function and are only presented to

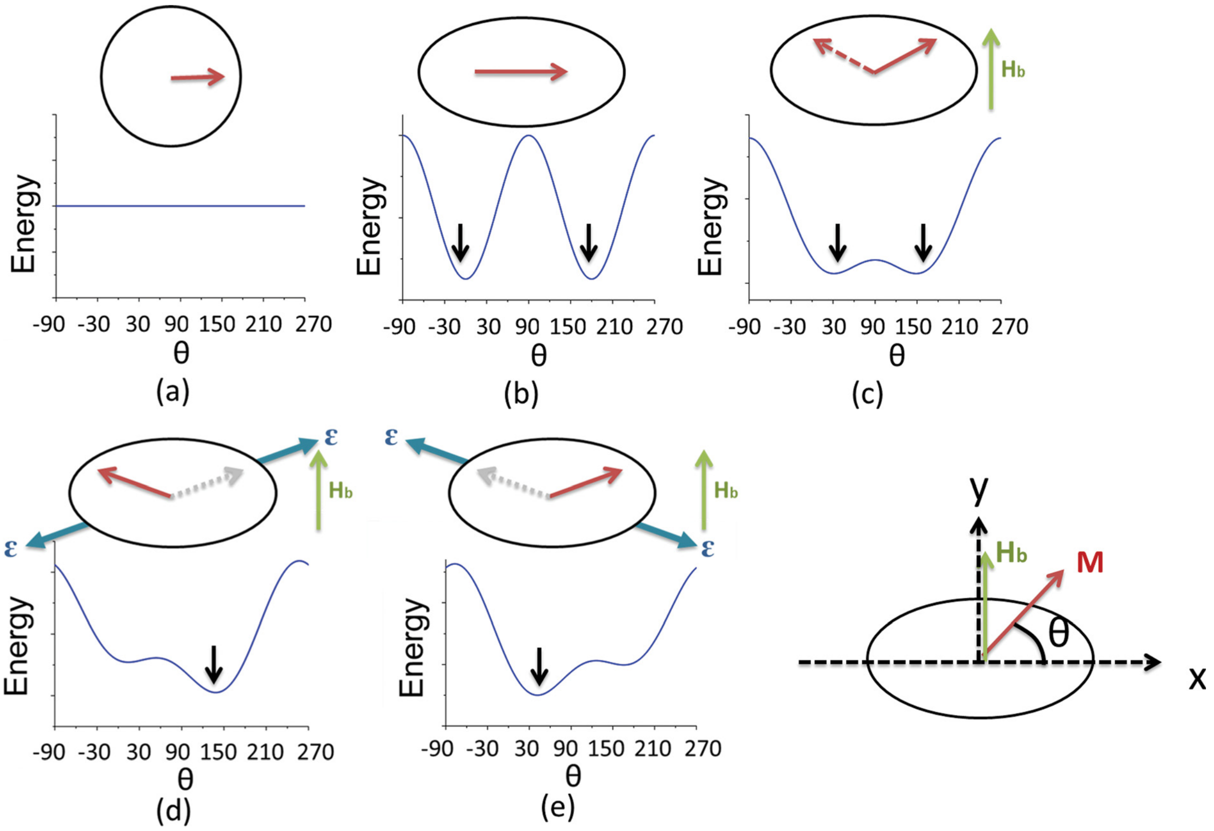

FIG. 1. An energetic diagrammatic description of the proposed memory element. (a) Circular disk: Isotropic shape in-plane. (b) Elliptical disk: shape anisotropic induced easy direction along the major axis of the ellipse (0 or 180). (c) Bias field effect: two stable states are generated by a bias field H_b. Energy barrier between two states is lowered by bias field H_b. (d) and (e) Interaction of shape anisotropy, bias field, and applied tensile strain, changing the energy profile ($+\theta$ or $-\theta$).

demonstrate the concept of single domain switching by 90° on a thin film PZT mounted to a Si substrate. Rather than model the entire substrate, the interface of the PZT with the Pt/Si interface is clamped to prevent displacement. As shown in the cross-section of Figure 2(b), the in-plane x-y dimensions have been reduced to 1000 × 1000 nm, and these boundaries along the x- and y-directions are also clamped to prevent displacements. In this model, voltage is always applied to two top Au

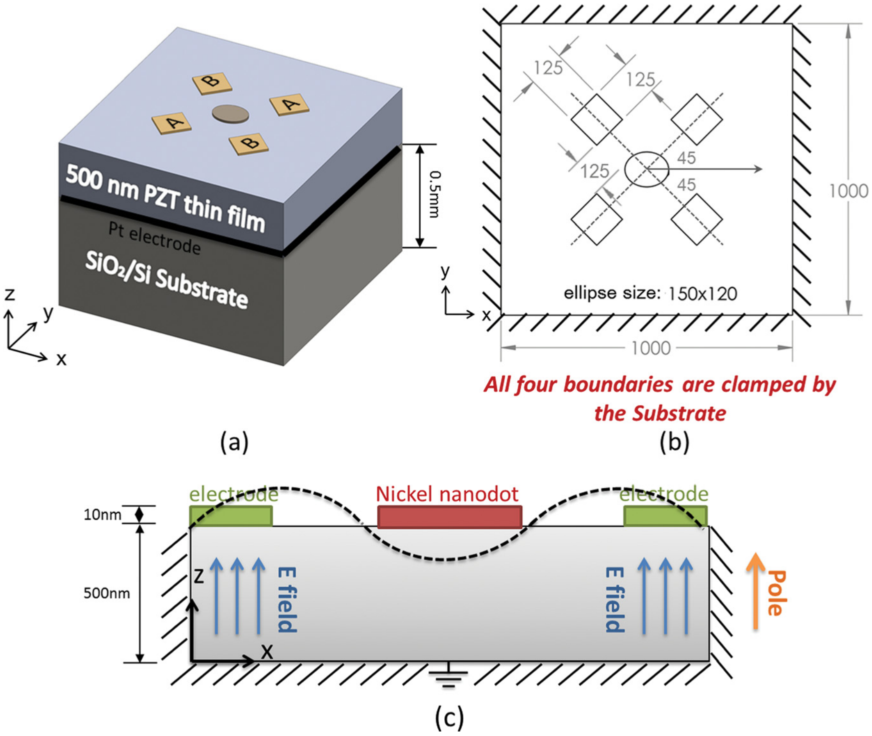

FIG. 2. Schematic of the bi-stable memory bit. (a) The memory bit consists of an elliptical ferromagnetic element deposited on a ferroelectric layer with patterned electrodes around the ferromagnetic element. (b) Schematic of top view, showing all four boundaries of the PZT thin film clamped by the Si substrate. (c) Cross-section view, showing mechanical response to applied electric field. By applying a positive voltage to the two electrode pairs (A-A), mechanical stretching is induced between the electrodes.

electrode sets (i.e., either A-A or B-B sets) with the bottom Pt electrode grounded; that is, the electric field is applied through the thickness of the PZT-5H. Figure 2(c) illustrates the deformation generated with the application of a voltage to produce a positive electric field. The d_{33} out-of-plane extension under the two sets of electrodes (e.g., A-A) generates an in-plane anisotropic tensile strain in the Ni nanodot, as illustrated with the dashed line. This local anisotropic strain switches the magnetic spin state of the Ni ellipse (or energy wells) between the two stable energy wells, as shown in Figures 1(d) and 1(e). The strain produced with this geometric configuration has been previously demonstrated on a bulk PZT sample, as described by Cui.[20] When the A-A electrodes are energized, the spins align along 45° direction; while if the B-B electrodes are energized, the spins align along 135°. Both angles represent stable equilibrium positions without a voltage/electric field applied.

The finite element model for Figure 2(a) is constructed as follows. The nickel properties are $M_s = 4.8 \times 10^5$ (A/m); $A_{ex} = 1.05 \times 10^{-11}$(J/m); $\lambda_{100} = -46 \times 10^{-6}$, $\lambda_{111} = -24 \times 10^{-6}$, $c_{11} = 2.5 \times 10^{11}$(N/m^2), $c_{12} = 1.6 \times 10^{11}$(N/m^2), and $c_{44} = 1.18 \times 10^{11}$(N/m^2).[28] The magnetocrystalline anisotropy energy term is an order of magnitude smaller than the magnetoelastic energy (i.e., soft ferromagnetic material) and is assumed negligible. The Gilbert damping constant was set as $\alpha = 0.5$ to improve stability and process time. The PZT-5H material properties are[35] $d_{33} = 5.93 \times 10^{-10}$(C/N); $d_{31} = -2.74 \times 10^{-10}$(C/N), $c_{11} = c_{22} = 1.27205 \times 10^{11}$(Pa), $c_{12} = 8.02122 \times 10^{10}$(Pa), $c_{13} = c_{23} = 8.46702 \times 10^{10}$(Pa), $c_{33} = 1.17436 \times 10^{11}$(Pa), $c_{44} = c_{55} = 2.29885 \times 10^{10}$(Pa), and $\rho = 7500$(kg/m^3). The Young's modulus and Poisson's ratio for Au are $E^{Au} = 7 \times 10^{10}$(N/m^2) and $\nu^{Au} = 0.44$, respectively.[35] The exchange length, defined as $\sqrt{\frac{2A_{ex}}{\mu_0 M_s^2}}$, is 8.5 nm for nickel. The nickel nanoellipse is discretized using tetrahedral elements with a size on the order of nickel's exchange length. The remainder of the structure (i.e., PZT-5H thin film, Au electrodes) is discretized using tetrahedral elements with graded element sizes dependent upon local geometry. The voltage used during this study is −0.5 V applied as a step function for $6\times\ 10^{-11}$ s on either electrodes A-A or B-B (electrical field through the thickness is 1 MV/m). That is, a voltage is applied for a period of time sufficiently long to allow spin equilibrium to be obtained, and the voltage is then removed. All simulations include a magnetic bias field applied along the minor axis of the nano-ellipse. Prior to application of the bias magnetic field or voltage, all magnetic spins are uniformly canted out of the x-y plane at 45° and allowed to precess toward an equilibrium state.

The first study determines the influence of magnitude bias field (Figures 1(b) and 1(c)) on the location of the magnetic energy wells. In this study, the same boundary conditions as described above were used, but the applied voltage is zero. Figure 3 plots the magnetic energy well location (see insert for angle definition) as a function of applied bias magnetic field. Figure 3 also includes results from a

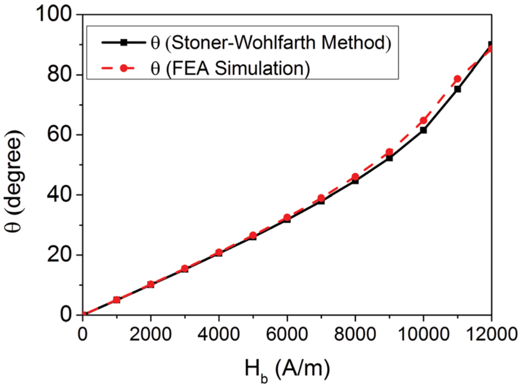

FIG. 3. The angle of the energy minima and energy barrier, comparing values obtained from Stoner-Wohlfarth (SW) calculation and present FEA simulation work, as a function of applied bias field.

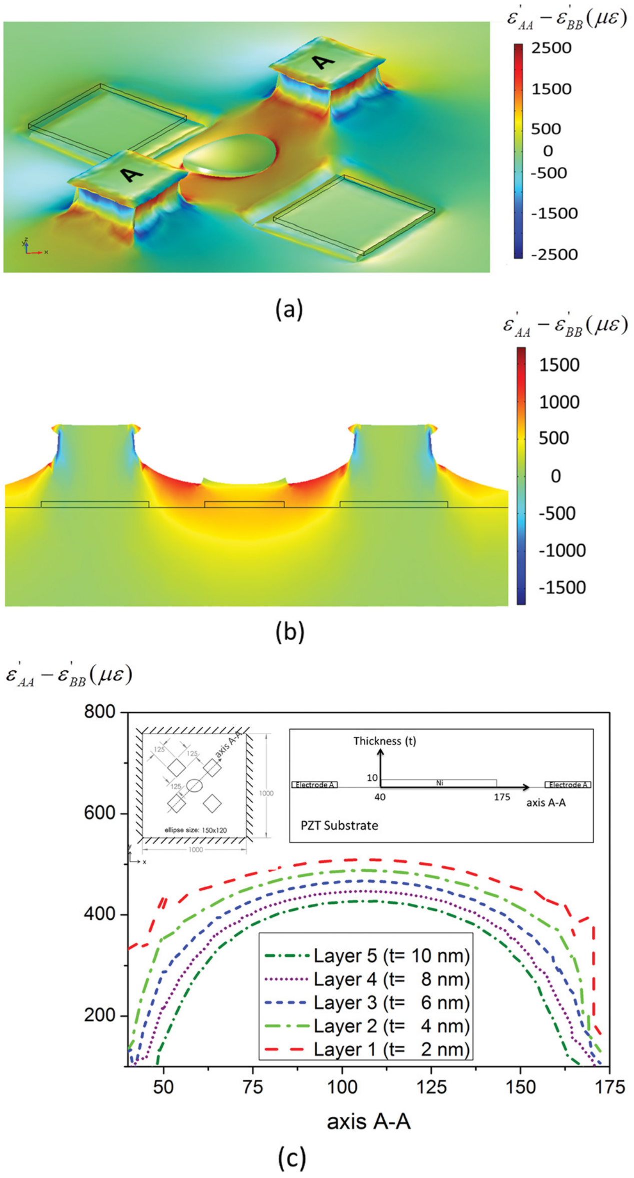

(a)

(b)

(c)

FIG. 4. Simulation results (displacement scale exaggerated) (a) Voltage applied on A-A electrode pair. Two electrodes expand out-of-plane and tensile strain is induced in the middle region. (b) Cross-section 2D plot along A-A. Tensile strain is induced in the middle (~800 $\mu\varepsilon$). The strain transferred to the nano-ellipse is ~450 $\mu\varepsilon$. Non-uniform strain distribution exists between the substrate and the nano-ellipse. (c) Strain for different layers in the nanoellipse along A-A.

Stoner-Wohlfarth model[30] with the finite element model. As the results show, as the magnetic field increases, the angle of the stable energy well increases and approaches 90°. While the Stoner-Wohlfarth and the finite element model are in good agreement when determining the location of the energy wells, the Stoner-Wohlfarth model does a poor job of predicting the combined magnetic/elastic response of this structure. To approach the angle pictorially represented in Figure 1(c), a constant bias field (H_b) of 9000 A/m is required to orient the magnetic energy wells at ~45° and ~135°. This value can be achieved using an antiferromagnetic exchange coupling layer.[38] The following simulations incorporate an $H_{b=}9000$ A/m.

Figure 4 shows results for $H_b = 9000$ A/m and -0.5 V applied to the A-A electrode pair. In Figure 4(a), a three-dimensional deformation plot along with relative strain contour plots ($\varepsilon'_{AA} - \varepsilon'_{BB}$) are presented. The terms ε'_{AA} and ε'_{BB} represent the normal strains along A-A and B-B axes, respectively. The contour plot indicates that the strain is limited to the region between electrodes A-A and does not significantly influence the surrounding region. Figure 4(b) provides a 2-D deformation plot along with relative strain contour plots for section A-A. The deformation is very similar to that presented in Figure 2(c). That is, the PZT beneath the electrodes expands out-of-plane. This expansion, in turn, generates tensile strain in the center region along the A-A direction. The contour strain plot shows that the anisotropic strain ($\varepsilon'_{AA} - \varepsilon'_{BB}$) in the Ni nanoellipse is on the order of 450 $\mu\varepsilon$ but is spatially distributed. To more closely examine the strain distribution, Figure 4(c) provides the anisotropic strain ($\varepsilon'_{AA} - \varepsilon'_{BB}$) as a function of position along the A-A direction (see insert). The five curves in the figure represent five different z locations through the thickness in the Ni nanoellipse. In general, the anisotropic strain decreases from the bottom (i.e., interface of PZT with Ni) to the top of the Ni nanoellipse. Also there is a significant reduction in strain near the edges of the Ni nanoellipse, $x = 40$ nm and 175 nm due to the shear lag effect. Shear lag effects become important and must be taken into account as the thickness of the magnetic layer increases relative to the minor axis dimension. At the top of the Ni ($t = 10$ nm), the strain near the edge (axis = 40 nm and 175 nm) is about 100 $\mu\varepsilon$, while the relative strain at the center (axis = 100 nm) is about 400 $\mu\varepsilon$. At the bottom of the Ni ($t = 2$ nm), the strain near the edge ($x = 40$ nm and 175 nm) is about 300 $\mu\varepsilon$ while the relative strain at the center ($x = 100$ nm) is about 500 $\mu\varepsilon$, which shows that the strain decreases through the thickness. The average strain transferred to the nanoellipse is approximately 450 $\mu\varepsilon$, representing a ~60% decrease in strain magnitude compared to material near the electrodes (~1000 $\mu\varepsilon$). The strain also decreases significantly in the Ni nanoellipse between two neighbors.

Figure 5 shows the magnetic response of the structure when either electrodes A-A (Figure 5(a)) or B-B (Figure 5(b)) are energized. The magnetization is initially in an equilibrium state at ~45° with respect to the x-axis. Electrodes A-A are initially energized as shown in Figure 5(a). The top figure shows the voltage applied and the magnetic dipole orientations in the Ni nanoellipse after equilibrium is reached. The larger arrow on the Ni nanoellipse is used to inform the reader of the magnetic spin states of each element. The bottom Figure 5(a) shows an exaggerated in-plane (x-y plane) deformation plot along with a relative strain contour plot ($\varepsilon'_{AA} - \varepsilon'_{BB}$). The deformation plot in this figure illustrates the stretching of the ellipse along the A-A direction that is consistent with the results shown in Figure 4. This stretching causes the magnetic spins in a negative magnetic material like Ni to rotate toward the stable equilibrium position located at ~135° (see Figures 1(d) and 1(e)) as shown in Figure 5(a). When the voltage is removed (not shown), the magnetic spins are stable at ~135° and do not return to ~45°. Following this voltage loading sequence, electrodes B-B are energized with results shown in Figure 5(b). As can be seen in the bottom of Figure 5(b), the displacement of the Ni nanoellipse is now along the B-B axis rather than along the A-A axis as shown in Figure 5(a). This stretching of the

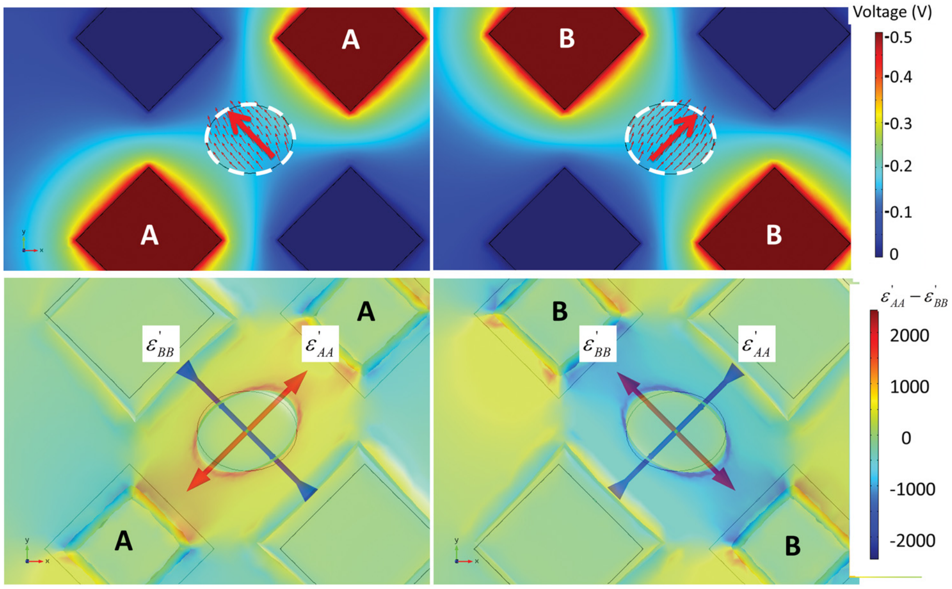

(a) (b)

FIG. 5. Top view of strain intensity plot from the fully coupled simulation results. (a) (Top) Magnetization rotates due to the application of strain from electrode pair (A-A). (Bottom) Applied voltage on A-A creating 45° tensile principle strain. (b) (Top) Magnetization rotates due to the application of strain from electrode pair (B-B). (Bottom) Applied voltage to B-B creating 135° tensile principle strain.

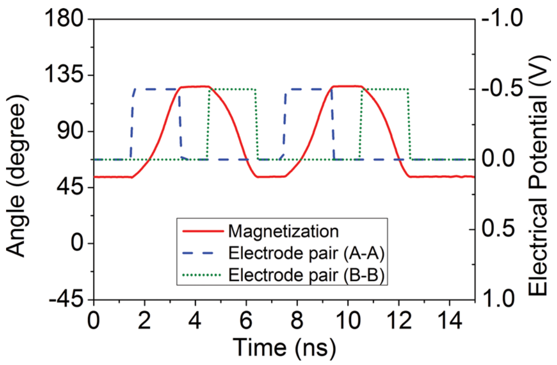

FIG. 6. Time response of the memory bit. The magnetization starts at zero and voltage is applied to electrode pair A-A, switching M to the "1" state; voltage on B-B switches M to the "0" state. The magnetization is bi-stable. The dashed blue line represents voltage applied to A-A; the dashed green line represents voltage applied to B-B; and the red line represents the response of the magnetization.

ellipse along B-B causes the magnetic spins to reorient along the A-A axis as shown in Figure 5(b) top with the large red arrow. Once the voltage is removed, the magnetic spins remain along the B-B axis since this is a stable equilibrium position (see Figure 1(d)).

Figure 6 shows magnetization and voltage applied as a function of time for the case presented in Figure 5. The blue dashed line is the voltage applied to A-A, the green dashed line is the voltage applied to B-B, and the red line is the average magnetization state. The left vertical axis corresponds to the magnetization direction (i.e., angle measured from x-axis) while the right vertical axis represents voltage. Initially the stable magnetic equilibrium is at ~45° when a voltage is applied to A-A at time = 1.5 ns and held until 3.5 ns. The magnetization responds at approximately 2 ns and switches from 45 to ~135 at 3 ns. The magnetization response time is approximately 1.5 ns. When the voltage (A-A) is removed, the magnetization remains in this new state, since it represents a stable equilibrium well. When the second pair (B-B) is energized at 4.5 ns, the magnetization rotates back to ~45°, and remains there following removal of the voltage to B-B. The electrical energy required to "write" (switch) this magnetic single domain can be calculated from the surface charge on the electrodes and the applied voltage. For the mechanism shown in Figures 5 and 6, the switching energy is approximately 80 fJ. This energy is associated with deformation of the PZT, strain in the electrodes, and strain in the Ni structure. This value is considered a conservative value, given that the structure has not been optimized with respect to PZT thickness or electrode size.

IV. CONCLUSION

This paper presented a robust analytical model combining micromagnetics with elastodynamics and electrostatics to solve a strain-mediated composite multiferroic problem. The solution was implemented in a finite element code providing both spatial and temporal information on the magnetic, electric, and mechanical fields. The problem of a single magnetic domain structure attached to a clamped piezoelectric thin film was studied. Analytical results demonstrate that out-of-plane deformations produce sufficient strain to reorient the magnetic structure, overcoming the classical substrate clamping problem. Work remains to be conducted on other magnetoelastic materials and optimizing the various structural geometries to minimize the required electrical energy to reorient or write this domain structure.[37]

ACKNOWLEDGMENTS

The authors would like to thank Kyle Wetzlar and Joshua Hockel for insightful discussions. This work was supported by NSF Nanosystems Engineering Research Center for Translational Applications of Nanoscale Multiferroic Systems (TANMS) Cooperative Agreement Award EEC-1160504.

[1] A. Roy, R. Gupta, and A. Garg, "Multiferroic memories," Adv. Condensed Matter Phys. **2012**, 926290.
[2] W. Eerenstein, M. Wiora, J. L. Prieto, J. F. Scott, and N. D. Mathur, "Giant sharp and persistent converse magnetoelectric effects in multiferroic epitaxial heterostructures," Nature Mater. **6**, 348–351 (2007).
[3] T. H. E. Lahtinen, K. J. A. Franke, and S. van Dijken, "Electric-field control of magnetic domain wall motion and local magnetization reversal," Sci. Rep. **2**, 258 (2012).
[4] N. Pertsev and H. Kohlstedt, "Resistive switching via the converse magnetoelectric effect in ferromagnetic multilayers on ferroelectric substrates," Nanotechnology **21**(47), 475202 (2010).
[5] J. M. Hu, Z. Li, L. Q. Chen, and C. W. Nan, "High-density magnetoresistive random access memory operating at ultralow voltage at room temperature," Nat. Commun. **2**, 553 (2011).
[6] J.-M. Hu, Z. Li, J. Wang, J. Ma, Y. H. Lin, and C. W. Nan, "A simple bilayered magnetoelectric random access memory cell based on electric-field controllable domain structure," J. Appl. Phys. **108**(4), 043909 (2010).
[7] K. Roy, S. Bandyopadhyay, and J. Atulasimha, "Switching dynamics of a magnetostrictive single-domain nanomagnet subjected to stress," Phys. Rev. B **83**(22), 224412 (2011).
[8] N. Tiercelin, Y. Dusch, V. Preobrazhensky, and P. Pernod, "Magnetoelectric memory using orthogonal magnetization states and magnetoelastic switching," J. Appl. Phys. **109**(7), 07D726 (2011).
[9] R. Ramesh and N. A. Spaldin, "Multiferroics: Progress and prospects in thin films," Nature Mater. **6**, 21–29 (2007).
[10] T. K. Chung, S. Keller, and G. P. Carman, Appl. Phys. Lett. **94**(13), 132501 (2009).
[11] T. K. Chung, K. Wong, S. Keller, K. L. Wang, and G. P. Carman, J. Appl. Phys. **106**(10), 103914 (2009).
[12] Z. Li, J. Wang, Y. Lin, and C. W. Nan, "A magnetoelectric memory cell with coercivity state as writing data bit," Appl. Phys. Lett. **96**(16), 162505 (2010).
[13] G. H. Dai, Q. F. Zhan, H. L. Yang, Y. W. Liu, X. S. Zhang, Z. H. Zuo, B. Chen, and R. W. Li, "Controllable strain-induced uniaxial anisotropy of Fe81Ga19 films deposited on flexible bowed-substrates," J. Appl. Phys. **114**, 173913 (2013).
[14] T. Wu, A. Bur, H. K. D. Kim, P. Zhao, and G. P. Carman, "Giant electrical control of magnetic anisotropy in magnetoelectric heterostructures using (011) PMN-PT single crystal," Proc. SPIE **7978**, 797818 (2011).
[15] T. Wu, A. Bur, P. Zhao, K. P. Mohanchandra, K. Wong, K. L. Wang, C. S. Lynch, and G. P. Carman, "Giant electric-field-induced reversible and permanent magnetization reorientation on magnetoelectric Ni/(011) [Pb(Mg1/3Nb2/3)O-3]((1-x))-[PbTiO3](x) heterostructure," Appl. Phys. Lett. **98**(1), 012504 (2011).
[16] Y. Wang, J. M. Hu, Y. H. Lin, and C. W. Nan, "Multiferroic magnetoelectric composite nanostructures," Npg Asia Mater. **2**, 61–68 (2010).
[17] N. Moutis, D. Suarez-Sandoval, and D. Niarchos, "Voltage-induced modification in magnetic coercivity of patterned $Co_{50}Fe_{50}$ thin film on piezoelectric substrate," J. Magn. Magn. Mater. **320**(6), 1050–1055 (2008).
[18] A. Bur, T. Wu, J. Hockel, C.-J. Hsu, H. K. D. Kim, T.-K. Chung, K. Wong, K. L. Wang, and G. P. Carman, "Strain-induced magnetization change in patterned ferromagnetic nickel nanostructures," J. Appl. Phys. **109**(12), 123903 (2011).

[19] F. Zavaliche, H. Zheng, L. Mohaddes-Ardabili, S. Y. Yang, Q. Zhan, P. Shafer, E. Reilly, R. Chopdekar, Y. Jia, P. Wright, D. G. Schlom, Y. Suzuki, and R. Ramesh, "Electric field-induced magnetization switching in epitaxial columnar nanostructures," Nano Lett. **5**(9), 1793–1796 (2005).

[20] J. Cui, J. L. Hockel, P. K. Nordeen, D. M. Pisani, C. Liang, G. P. Carman, and C. S. Lynch, "A method to control magnetism in individual strain-mediated magnetoelectric islands," Appl. Phys. Lett. **103**(23), 232905 (2013).

[21] T. L. Gilbert, "A phenomenological theory of damping in ferromagnetic materials," IEEE Trans. Magn. **40**, 3443–3449 (2004).

[22] B. Zhu, C. C. H. Lo, S. J. Lee, and D. C. Jiles, "Micromagnetic modeling of the effects of stress on magnetic properties," J. Appl. Phys. **89**(11), 7009 (2001).

[23] R. Hu, A. Soh, G. Zheng, and Y. Ni, "Micromagnetic modeling studies on the effects of stress on magnetization reversal and dynamic hysteresis," J. Magn. Magn. **301**, 458–468 (2006).

[24] N. D'Souza, J. Atulasimha, and S. Bandyopadhyay, "Four-state nanomagnetic logic using multiferroics," J. Phys. D. Appl. Phys. **44**(26), 265001 (2011).

[25] Y. C. Shu, M. P. Lin, and K. C. Wu, "Micromagnetic modeling of magnetostrictive materials under intrinsic stress," Mech. Mater. **36**(10), 975–997 (2004).

[26] J. X. Zhang and L. Q. Chen, "Phase-field microelasticity theory and micromagnetic simulations of domain structures in giant magnetostrictive materials," Acta Mater. **53**(9), 2845–2855 (2005).

[27] B. D. Cullity and C. D. Graham, *Introduction to Magnetic Materials*, 2nd ed. (Wiley-IEEE Press, 2008).

[28] R. C. O'Handley, *Modern Magnetic Materials: Principles and Applications*, 1st ed. (Wiley-Interscience, 1999).

[29] L. Bañas, "Adaptive techniques for Landau–Lifshitz–Gilbert equation with magnetostriction," J. Comput. Appl. Math. **215**(2), 304–310 (2008).

[30] E. C. Stoner and E. P. Wohlfarth, Philos. Trans. R. Soc. **A240**, 599 (1948).

[31] D. R. Fredkin and T. R. Koehler, "Hybrid method for computing demagnetizing fields," IEEE Trans. Magn. **26**(2), 415–417 (1990).

[32] H. Szambolics, L. D. Buda-Prejbeanu, J. C. Toussaint, and O. Fruchart, "Innovative weak formulation for the Landau-Lifshitz-Gilbert equations," Comput. Mater. Sci. **44**, 253 (2008).

[33] A. Weddemann, D. Kappe, and A. Hutten, *COMSOL Conference, Boston, MA* (2011).

[34] F. Alouges and P. Jaisson, "Convergence of a finite element discretization for the Landau–Lifshitz equations in micromagnetism," Math. Mod. Methods Appl. Sci. **16**, 299 (2006).

[35] See http://www.comsol.com/ for COMSOL Multiphysics.

[36] J. Dean, M. T. Bryan, G. Hrkac, A. Goncharov, C. L. Freeman, M. A. Bashir, T. Schrefl, and D. A. Allwood, "The incorporation of the Cauchy stress matrix tensor in micromagnetic simulations," J. Appl. Phys. **108**, 073903 (2010).

[37] K. Roy, S. Bandyopadhyay, and J. Atulasimha, "Energy dissipation and switching delay in stress-induced switching of multiferroic nanomagnets in the presence of thermal fluctuations," J. Appl. Phys. **112**, 023914 (2012).

[38] V. Laukhin, V. Skumryev, X. Martí, D. Hrabovsky, F. Sánchez, M. V. García-Cuenca, C. Ferrater, M. Varela, U. Lüders, J. F. Bobo, and J. Fontcuberta, "Electric-field control of exchange bias in multiferroic epitaxial heterostructures," Phys. Rev. Lett. **97**, 227201 (2006).